A&A 525, L5 (2011)
DOI: 10.1051/0004-6361/201015743

Astronomy & Astrophysics

Letter to the Editor

The origin of palladium and silver⋆

C. J. Hansen and F. Primas

European Southern Observatory (ESO), Karl-Schwarschild-Str. 2, 85748 Garching b. München, Germany
e-mail: [cjhansen;fprimas]@eso.org

Received 12 September 2010 / Accepted 24 October 2010

ABSTRACT

Context. In recent years, progress has been made in understanding the rapid neutron-capture process (*r*-process) and current studies suggest the need for a second, so-called weak *r*-process. Observational proof of this possible second branch of the *r*-process may come from a detailed knowledge of the formation and evolution of silver (Ag) and to some extent palladium (Pd) abundances in halo stars.
Aims. We study the silver and palladium abundances of a large sample of stars (only a few measurements have been made so far) to gain insight into the formation process of lighter neutron-capture elements.
Methods. We analysed a sample of stars (including both dwarfs and giants), for which we determined in a consistent manner stellar parameters and abundances. The abundances were derived via spectrum synthesis, making use of the MOOG synthetic spectrum code (1D LTE) and MARCS stellar model atmospheres (1D LTE).
Results. We derived the Ag and Pd abundances of 56 stars, the largest sample to date for which both Pd and Ag have been studied. The stars span a metallicity range of 2.5 dex, from the metal-poor giants at [Fe/H] ~ -3.2 to the more metal-rich dwarfs at [Fe/H] ~ -0.6. Both elements display rather flat trends with metallicity, with some dispersion being present at the lowest metallicities.
Conclusions. The similarity detected in the evolutionary trends of both Ag and Pd is indicative of a common origin. Qualitative comparisons with some theoretical calculations seem to confirm the need for a second *r*-process, responsible for their formation. Further abundance studies (exploring more light n-capture elements) and comparisons with a wider variety of theoretical models are needed to fully characterise the details and site of the formation mechanism(s).

Key words. stars: abundances – nuclear reactions, nucleosynthesis, abundances

1. Introduction

The study of the chemical evolution of the Galaxy relies not only on accurate determination of chemical abundances, but also on a solid understanding of the different nucleosynthesis processes responsible for the formation of the different elements. Apart from the very light species (from hydrogen to boron) that formed during the Big Bang or follow from spallation reactions, elements in the Periodic Table up to $Z \sim 30$ form via fusion in stars. Charged particle processes work well up to the iron-peak, beyond which further fusion becomes energetically too demanding. Formation of heavier elements requires extra energy, iron-peak seeds (as well as neutrons), and available production channels. These channels are mainly neutron-capture processes, which play a major role in the production of what we commonly call "heavy" elements ($Z > 30$). Depending on the number of available neutrons, the processes take place on different timescales. At relatively low ($\simeq 10^8$ cm^{-3}) neutron densities (Kappeler et al. 1989; Busso et al. 1999), a long duration process will take place, whereas in environments with higher ($n_n \sim 10^{26}$ cm^{-3}) neutron densities (Kratz et al. 2007) a shorter one will exist. These two scenarios correspond to the so-called *slow* and *rapid* neutron-capture processes (*s*- and *r*-, respectively).

Nature, however, is more complex than this and both these processes appear to have multiple components. The main component of the *s*-process is linked to both thermally pulsating asymptotic giant branch (AGB) and red giant branch (RGB) stars with stellar masses in the range 1.5 to 8 $M_\odot$ (Sneden et al. 2008) yielding nuclei with atomic masses $90 \leq A \leq 209$ (Heil et al. 2009). This process is generally associated with carbon-rich environments and the neutrons are a by-product of ^{13}C reactions. The weak component, instead, takes place in more massive stars ($M \geq 8\ M_\odot$), during their He core burning phase, and the neutrons come primarily from ^{22}Ne reactions. This component is responsible for the formation of lighter elements ($56 \leq A \leq 90$) (Heil et al. 2009; Pignatari et al. 2010).

Supernovae (SN) offer higher neutron densities than AGB stars, thus SN have been identified as one of the possible sites for the origin of the *r*-process. However, this process is not yet very well understood. Several sites have been suggested and investigated: neutron star mergers (Freiburghaus et al. 1999), high mass supernova (Wasserburg & Qian 2000), neutrino-driven winds (Wanajo et al. 2001), low mass O-Ne-Mg SN (Wanajo et al. 2003), core-collapse SN (Argast et al. 2004), and high-entropy winds (Farouqi et al. 2010), but without reaching a firm conclusion. Recent studies (Burris et al. 2000; Sneden et al. 2003; François et al. 2007; Montes et al. 2007) have suggested that this process may also work via two distinct channels, depending on the neutron density of the surrounding environment: high *n*-density regions would be connected to the main component,

⋆ Appendix is only available in electronic form at http://www.aanda.org

whereas lower n-densities ($\sim 10^{20}$ cm^{-3}, Kratz et al. 2007) would favour the so-called weak r-process (Wanajo et al. 2001) (or a second r-process) and be responsible for the formation of the $40 \leq Z \leq 47$ elements in low metallicity environments. Montes et al. (2007) identified the upper end of this range as the possible key to prove the existence and eventually characterise the second r-process component, but so far these elements (Mo, Pd and Ag) have scarcely been studied.

This has triggered our fresh look into this rather unexplored area of the Periodic Table, to derive accurate abundances of the light n-capture elements, focusing on silver (Ag, $Z = 47$) and palladium (Pd, $Z = 46$). Very little can be found in the literature about these elements, with several studies having analysed only one object each (Cowan et al. 2002; Hill et al. 2002; Sneden et al. 2003; Honda et al. 2006) and only a couple of studies having analysed slightly larger samples (Crawford et al. 1998; Johnson & Bolte 2002, respectively, 7 and 3 stars).

For palladium, the situation is slightly better, but we are still in the low number statistics regime. Most of the Pd abundances in the literature come from single-star investigations, with only Johnson & Bolte (2002) having analysed palladium in 12 stars. However, out of these 12, only three are detections.

To investigate the underlying formation process of these elements, a larger sample is needed to draw firmer conclusions. Both silver and palladium have their main resonant transitions in the same near-UV part of our spectra (Ag I: 328.07 nm and 338.29 nm; Pd I: 340.45 nm), so that we have been able to study both of them in the same stars and in a consistent manner.

2. Observations and data reduction

Our sample includes 33 dwarfs, all observed by ourselves with UVES (Dekker et al. 2000) at the VLT, and 23 giants, observed with UVES and HIRES (Vogt et al. 1994) at Keck, most of which were retrieved from the VLT and Keck archives. The sample spans a broad range in temperature, gravity, and metallicity. All spectra are of high quality, being characterised by $R \geq 40\,000$ and signal-to-noise ratios between 100 and 150 (at 340 nm). A few of the giants are r-process-rich stars (see Table 1).

We reduced all dwarf star UVES spectra with the UVES pipeline (v. 4.3.0) and IRAF[1], while for the giants we worked directly on the reduced spectra readily available from the respective archives, after having carefully inspected them. All spectra were then shifted to the rest frame and coadded, and their continua normalized.

3. Method and analysis

Silver and palladium have their main resonant transitions in the near-UV, at respectively 328.0 nm and 338.2 nm, and at 340.4 nm. Owing to the severe crowding of these spectral regions and to the presence of blends affecting the bluest of the two Ag lines, we derived both Ag and Pd abundances via spectrum synthesis, using MARCS 1D model atmospheres (Gustafsson et al. 2008) and the MOOG spectrum synthesis code (Sneden 1973, 2009) under LTE assumptions. Only the metallicity of our stars was derived from equivalent width measurements (see below), but using the same model atmospheres and code.

A full description of our analysis will be presented in a forthcoming paper (Hansen et al., in prep.), which will present the complete analysis of heavy elements in the entire sample; here, we briefly summarise only the most important steps of our determinations.

Table 1. Stellar parameters, and silver and palladium abundances of our dwarf and giant stars. The complete table is available online.

Star	$T_{\rm eff}$	log g	[Fe/H]	Vt	[Pd/Fe]	[Ag/Fe]
Dwarfs						
HD 3567	6035	4.08	–1.33	1.5	0.29	0.53
HD 19445	5982	4.38	–2.13	1.4	0.12	–
HD 22879	5792	4.29	–0.95	1.2	0.17	0.00
...	...	...	...	...	...	...

3.1. Stellar parameters

We derived the stellar parameters for most of our sample stars applying colour-$T_{\rm eff}$ calibrations for the effective temperatures (Alonso et al. 1996, 1999), Hipparcos parallaxes for the gravities, and equivalent width measurements of Fe I lines for the metallicity (too few Fe II lines could be detected in the most metal-poor stars). For those stars with missing photometry or uncertain reddening values $E(B-V)$, we had to resort to deriving their effective temperatures based on their excitation potential, whereas for those stars with inaccurate parallaxes, we had to constrain their gravities via the ionization balance. The microturbulence velocity was constrained by requiring that all Fe I lines give the same abundance, irrespective of their strength.

The derivation of stellar parameters was performed iteratively. We derived typical uncertainties of ±100 K in effective temperatures (150 K when the excitation potential was used), ±0.2 dex in the gravities, ±0.15 dex in metallicity, and ±0.15 km s^{-1} in the microturbulence. Table 1 summarizes all stellar parameters for our sample stars.

3.2. Silver and palladium line lists

For both elements, we mainly used VALD[2] and Kurucz[3] molecular databases as our main sources of information on all atomic and molecular lines present in this spectral region. Some adjustments to the oscillator strengths of some of the neighbouring lines were applied (when applicable to a large number of spectra) to improve our best-fit syntheses.

Silver has two observable lines. The strongest line is at 328.068 nm and is blended with several other elements (Fe, Zr and Mn), making the feature more complex to analyse. The second (weaker) line is found at 338.289 nm and is less affected by blends. In collaboration with H. Hartmann (from the Atomic Physics Laboratory in Lund, priv. comm.), we carefully checked and re-compiled the line list for the silver lines, which now includes revised values of the hyperfine structure of both lines and new *hfs* levels, when compared to the older calculations by Ross & Aller (1972). With this line list, we derived a mean silver solar abundance of log $\epsilon(\mathrm{Ag})_\odot = 0.93$, which is in very good agreement with the 0.94 value derived by Asplund et al. (2009).

Our palladium abundances are based on one line at 340.45 nm, the log gf of which was taken directly from VALD. We derived a palladium solar abundance of log $\epsilon(\mathrm{Pd})_\odot = 1.52$, once again in good agreement with the 1.57 value derived by

[1] IRAF is distributed by the National Optical Atronomy Observatory, which is operated by the Association of Universities of Research in Astronomy, Inc., under contract with the National Science Foundation.

[2] Vienna Atomic Lines Database, available at http://vald.astro.univie.ac.at/vald/php/vald.php

[3] http://kurucz.harvard.edu/linelists

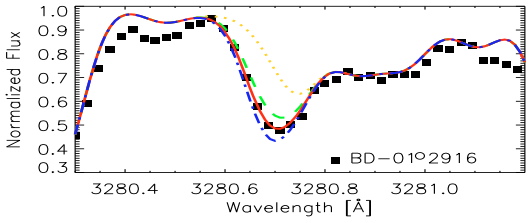

Fig. 1. Our best-fit spectrum synthesis of the Ag I 328.0 nm line in the metal-poor giant BD –01° 2916. Symbols and lines are as follows: filled squares – observed spectrum; solid red line – best-fit synthesis computed for [Ag/Fe] = −0.12; dotted yellow line – synthesis computed without silver, dashed green, and dot-dashed blue lines – syntheses computed, respectively, for [Ag/Fe] = −0.3 and +0.05.

Asplund et al. (2009). Independently of this good agreement, we used the Asplund et al. (2009) solar values throughout the paper, because we consider them to be more robust determinations. Further details about the line lists (including the revised line list for Ag) will be presented and discussed in Hansen et al. (in prep.).

4. Abundance results

With the stellar parameters reported in Table 1 and the line lists described above, we then synthesized the regions around the Ag lines and the Pd line. Our derived abundances are listed in the last two columns of the same Table 1. For silver, the reported values correspond to the mean value of the abundances derived from both lines, which agree to within 0.1 dex in 70% of the cases. Figure 1 shows one example of a best-fit spectrum synthesis, for the metal-poor ([Fe/H] = −2.0) giant star BD −01°2916.

The uncertainty due to systematic changes in the stellar parameters amounts to ±0.22 dex for our Ag abundances and ±0.18 dex for our Pd abundances. To these values, one then needs to add ±0.05 dex due to the uncertainty in placing the continuum, and ±0.1 dex, which we estimated to be our uncertainties in the syntheses (unknown lines, models, codes). After propagating all uncertainties, we have estimated total uncertainties of the order of 0.25 dex and 0.2 dex for our Ag and Pd abundances, respectively.

In Fig. 2, we show our derived values of [Pd/Fe] and [Ag/Fe] plotted versus [Fe/H]. Both plots show rather flat trends, with [Pd/Fe] at a level of ≃0.21 dex and [Ag/Fe] at a level of ≃0.18 dex. The dwarfs and giants samples seem to overlap rather well (with the possible exceptions of a few giants in the case of silver), but both evolutionary trends are affected by some dispersion, especially towards the lowest metallicities. The dispersion seems to be real: it is clearly larger than our estimated uncertainties, and cannot be accounted for by the few *r*-process enriched stars present in our sample. Only the two extremely *r*-process-rich stars in our sample fall on the upper envelope of both elemental trends: CS 22892-052 (Sneden et al. 2003) is slightly above the mean trend (filled triangle), whereas CS 31082-001 (Hill et al. 2002) confirms its different signature of light n-capture elements compared to CS 22892-052. As a matter of fact, for both Ag and Pd trends, CS 31082-001 identifies the top end of our abundances range.

After comparing our derived abundances to other literature studies, we found overall satisfactory agreement. Our Ag abundances agree to within the combined errors with the abundances derived by Crawford et al. (1998), and to a lesser extent to Johnson & Bolte (2002). A very good agreement is found for the Ag abundance of CS 31082-001 between ourselves and Hill et al. (2002). The lack of a metallicity dependence in the Ag trend

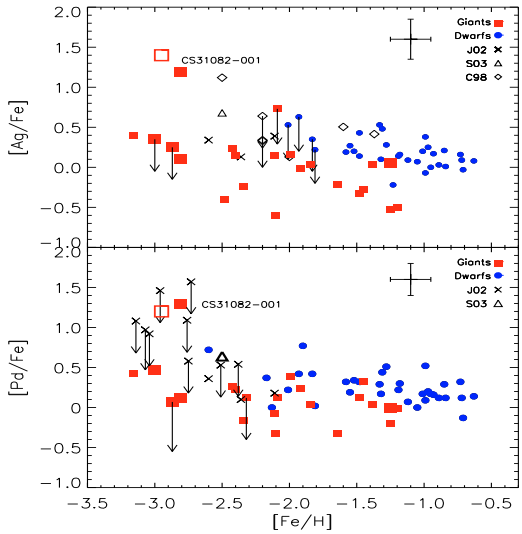

Fig. 2. [Pd/Fe] and [Ag/Fe] vs. [Fe/H]. Dwarfs are indicated as blue filled circles and giants as red filled squares. The larger filled red squares correspond to *r*-process enhanced stars. Comparison samples are plotted as well Crawford et al. (1998) -C98- filled diamonds, Johnson & Bolte (2002) -J02- ×-es (mainly upper limits) and Sneden et al. (2003) -S03- filled triangles. The open, red square corresponds to HE 1523-0901 (Frebel et al. 2007).

also confirms the earlier finding by Crawford et al. (1998), but is based on a much larger data sample.

A similar comparison for palladium is more complex, because most of the abundances derived by Johnson & Bolte (2002) are upper limits. We note however that their three detections would fall on our average [Pd/Fe] trend.

When we compare [Ag/H] to [Pd/H] (see Fig. 3), we find a clear correlation. Detailed χ^2 fits to our data samples show that the best-fit slope of the giants trend is 0.81, whereas the slope for the dwarfs trend is slightly shallower at 0.74. Both slopes indicate that the amount of Pd grows slightly faster than Ag, and this tendency becomes more pronounced as we move towards higher metallicities. This finding agrees well with Pd also being produced by the *s*-process, to a larger extent than Ag, hence its faster growth at higher metallicities.

In principle, a difference between Ag and Pd could also be accounted for by the so-called odd-even effect ($Z_{\rm Ag}$ = 47 and $Z_{\rm Pd}$ = 46), which would imply a different nucleosynthetic history. The amount, however, by which the mean abundances of Ag and Pd differ in our stars is very small and fully explained by observational errors. Therefore, this similarity in the evolutionary trends of Ag and Pd strongly suggests similar formation processes of these elements.

To fully understand this process, further comparisons to other elemental abundances, to SN yields, and to galactic chemical evolution models are needed. Wind model predictions (Kratz et al. 2007; Farouqi et al. 2010) illustrate that elements with mass numbers $A \simeq 100$–130 require too large entropies to be produced by charged particle processes, whereas a given neutron-to-seed ratio and intermediate entropies can yield the expected amount. This is indeed confirmed by the satisfactory fit we find by comparing the abundances derived for four stars of our sample to the predictions from the high entropy wind (HEW) parameter study by Kratz et al. (2007) and Farouqi et al. (2010). For this comparison, we used their predicted yields calculated for $Y_{\rm e}$ = 0.45, $V_{\rm wind}$ = 7500 km s^{-1}, varying entropy (S), and neutron-to-seed ratio ($Y_n/Y_{\rm seed}$). Figure 4 shows that the best fit (solid line) for all four stars is found with a model computed with an entropy $S \sim 125\,k_B$/baryon, which corresponds to $Y_n/Y_{\rm seed} \sim 5$,

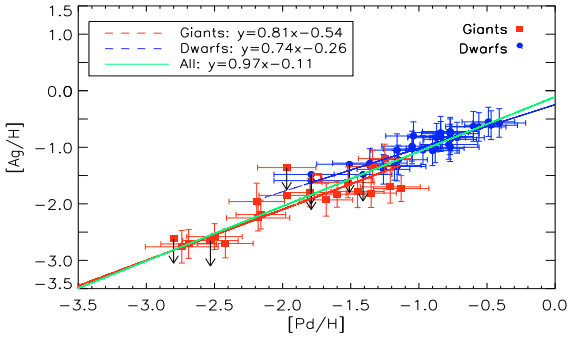

Fig. 3. [Ag/H] vs. [Pd/H]. Legend as in Fig. 2 and various line fittings. Fits to dwarfs are blue (dashed) and to giants are red (solid). The fit to all stars is a green (solid) straight line. The line provides a good fit to all stars, even the very *r*-process enhanced stars such as CS 31082-001 and HE 1523-0901.

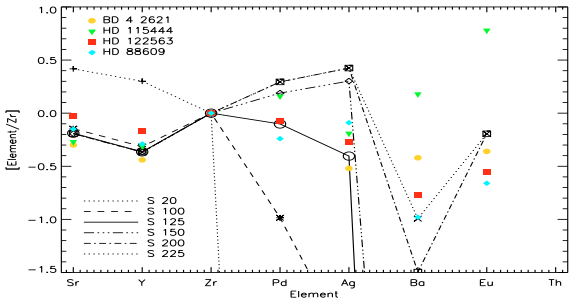

Fig. 4. [Element/Zr] ratios for four of our stars (see legend for filled, coloured symbols) compared to HEW yields calculated with varying entropies (S, see legend).

definitely in the weak *r*-process regime, where there are enough free neutrons for an *r*-process to occur. In this kind of wind scenario, lighter n-capture elements (such as Sr, Y, and Zr) would be produced by charged particle processes, while heavier elements (such as Eu) would result from the main *r*-process, which requires much higher entropies and neutron-to-seed ratios than Ag and Pd. Although qualitative, this comparison reinforces the need for a second *r*-process, in addition to the main *r*-process. This second process could be a weak *r*-process, which creates elements like Ag and Pd, with entropies around 125 k_B/baryon and intermediate neutron-to-seed ratios. However, its full characterisation clearly needs thorough comparisons with a larger suite of theoretical predictions (assuming a constant velocity and neutron volume density may not be a realistic choice for a SN wind) and a larger set of elemental abundances (more n-capture elements). These comparisons will be presented and discussed in Hansen et al. (in prep.).

5. Conclusions

To derive accurate abundances of Ag and Pd in halo stars, high resolution spectra of high signal-to-noise ratio are mandatory. Our sample includes 56 dwarf and giant stars, spanning a large range of metallicities, which were observed with two of the most efficient (in the near-UV) high-res spectrographs currently available (UVES and HIRES). Our analysis has focused on the derivation of silver and palladium abundances, two poorly studied elements that may hold important clues to the existence and nature of a second *r*-process.

Between the two, silver is clearly the best choice to investigate the existence of a second (weak) *r*-process, being mostly created by the *rapid* n-captures (80%, see Arlandini et al. 1999), whereas both *r*- and *s*-process nucleosyntheses contribute to the production of Pd (in almost a 50/50 ratio for the Sun).

The abundance trends we have derived are very similar for Ag and Pd, which implies that a similar process is responsible for their formation. This conclusion is reinforced by our lack of detection of any considerable odd-even effect.

Both Ag and Pd evolutionary trends are rather flat, with giants and dwarfs clearly overlapping but characterised by real dispersion. Furthermore, the Ag abundances correlate well with the Pd abundances (for both giants and dwarfs), with the Ag abundances growing slightly more slowly than the Pd abundances. This is most likely due to the mixed (*r*+*s*) nature of Pd, with the contribution from the *s*-process expected to increase with metallicity.

A qualitative comparison of our Ag and Pd abundances to the theoretical yields of high entropy winds (HEW) models strengthen the need for a second (weak) *r*-process responsible for their formation. Additional insights into the formation process and site of occurrence will be obtained by comparing Ag and Pd to other n-capture elements as well as to several site-dependent model predictions. These findings will be presented in our forthcoming paper (Hansen et al., in prep.).

Acknowledgements. This work was supported by ESO. CJH thanks Henrik Hartmann for providing new *hfs* calculations for Ag, Norbert Christlieb and Christopher Sneden for sharing spectra and Karl-Ludwig Kratz for sending yield predictions of HEW models and for interesting discussions. A special thank you goes to Oliver Hallman for useful discussions and clarifications. The authors thank the referee for useful comments and for suggesting to add HE1523-0901 to our analysis.

References

Alonso, A., Arribas, S., & Martinez-Roger, C. 1996, A&A, 313, 873
Alonso, A., Arribas, S., & Martínez-Roger, C. 1999, A&AS, 140, 261
Argast, D., Samland, M., Thielemann, F., & Qian, Y. 2004, A&A, 416, 997
Arlandini, C., Käppeler, F., Wisshak, K., et al. 1999, ApJ, 525, 886
Asplund, M., Grevesse, N., Sauval, A. J., & Scott, P. 2009, ARA&A, 47, 481
Burris, D. L., Pilachowski, C. A., Armandroff, T. E., et al. 2000, ApJ, 544, 302
Busso, M., Gallino, R., & Wasserburg, G. J. 1999, ARA&A, 37, 239
Cowan, J. J., Sneden, C., Burles, S., et al. 2002, ApJ, 572, 861
Crawford, J. L., Sneden, C., King, J. R., Boesgaard, A. M., & Deliyannis, C. P. 1998, AJ, 116, 2489
Dekker, H., D'Odorico, S., Kaufer, A., Delabre, B., & Kotzlowski, H. 2000, in SPIE Conf. Ser.
Farouqi, K., Kratz, K., Pfeiffer, B., et al. 2010, ApJ, 712, 1359
François, P., Depagne, E., Hill, V., et al. 2007, A&A, 476, 935
Frebel, A., Christlieb, N., Norris, J. E., et al. 2007, ApJ, 660, L117
Freiburghaus, C., Rosswog, S., & Thielemann, F. 1999, ApJ, 525, L121
Gustafsson, B., Edvardsson, B., Eriksson, K., et al. 2008, A&A, 486, 951
Heil, M., Juseviciute, A., Käppeler, F., et al. 2009, PASA, 26, 243
Hill, V., Plez, B., Cayrel, R., et al. 2002, A&A, 387, 560
Honda, S., Aoki, W., Ishimaru, Y., Wanajo, S., & Ryan, S. G. 2006, ApJ, 643, 1180
Johnson, J. A., & Bolte, M. 2002, ApJ, 579, 616
Kappeler, F., Beer, H., & Wisshak, K. 1989, Rep. Prog. Phys., 52, 945
Kratz, K., Farouqi, K., Pfeiffer, B., Truran, J. W., Sneden, C., & Cowan, J. J. 2007, ApJ, 662, 39
Montes, F., Beers, T. C., Cowan, J., Elliot, T., Farouqi, K., Gallino, R., Heil, M., Kratz, K., Pfeiffer, B., Pignatari, M., & Schatz, H. 2007, ApJ, 671, 1685
Pignatari, M., Gallino, R., Heil, M., Wiescher, M., Käppeler, F., Herwig, F., & Bisterzo, S. 2010, ApJ, 710, 1557
Ross, J. E. & Aller, L. H. 1972, Sol. Phys., 25, 30
Sneden, C., Cowan, J. J., Lawler, J. E., et al. 2003, ApJ, 591, 936
Sneden, C., Cowan, J. J., & Gallino, R. 2008, ARA&A, 46, 241
Vogt, S. S., Allen, S. L., Bigelow, B. C., et al. 1994, in SPIE Conf. Ser.
Wanajo, S., Kajino, T., Mathews, G. J., & Otsuki, K. 2001, ApJ, 554, 578
Wanajo, S., Tamamura, M., Itoh, N., et al. 2003, ApJ, 593, 968
Wasserburg, G. J., & Qian, Y. 2000, ApJ, 529, L21

Appendix A: Online material

Table A.1. Stellar parameters, and silver and palladium abundances for all our dwarf and giant stars.

Star	$T_{\rm eff}$	log g	[Fe/H]	Vt	[Pd/Fe]	[Ag/Fe]
Dwarfs						
HD 3567	6035	4.08	–1.33	1.5	0.29	0.53
HD 19445	5982	4.38	–2.13	1.4	0.12	–
HD 22879	5792	4.29	–0.95	1.2	0.17	0.00
HD 25704	5700	4.18	–1.12	1.0	0.07	0.09
HD 63077	5629	4.15	–1.05	0.9	0.00	0.07
HD 63598	5680	4.16	–0.99	0.9	0.09	–0.07
HD 76932	5905	4.08	–0.97	1.3	0.20	0.25
HD 103723	6128	4.28	–0.85	1.5	0.29	0.21
HD 105004	5900[a]	4.30	–0.84	1.1	0.12	0.01
HD 106038[b]	5950	4.33	–1.48	1.1	0.14	0.07
HD 111980[b]	5653	3.90	–1.32	1.15	0.17	0.05
HD 113679	5759	4.04	–0.63	0.9	0.14	0.08
HD 116064	5999	4.33	–2.17	1.5	0.37	–
HD 120559	5411	4.74	–1.33	0.7	0.44	0.48
HD 121004	5711	4.46	–0.73	0.65	0.34	0.16
HD 122196	6048	3.89	–1.81	1.2	0.02	<0.22
HD 126681[b]	5532	4.58	–1.28	0.6	0.51	0.28
HD 132475	5838	3.90	–1.52	1.5	0.34	0.20
HD 160617	6028	3.79	–1.83	1.3	0.42	<0.35
HD 166913[b]	6155	4.07	–1.93	1.5	0.42	<0.63
HD 175179[b]	5758	4.16	–0.72	0.9	0.12	0.09
HD 188510	5536	4.63	–1.58	1.0	0.32	0.19
HD 189558	5712	3.79	–1.18	1.2	0.40	0.16
HD 195633	6005	3.86	–0.71	1.4	–0.13	–0.03
HD 205650	5842	4.49	–1.19	0.9	0.22	0.14
HD 213657	6208	3.78	–2.01	1.2	0.22	<0.53
HD 298986	6144	4.18	–1.48	1.4	0.32	0.43
CD-33°3337	5952	3.95	–1.55	1.4	0.19	0.27
CD-45°3283	5657[c]	4.97	–0.99	0.8	0.52	0.38
CD-57°1633	5907	4.26	–1.01	1.1	0.17	0.20
G005-040	5766	4.23[a]	–0.93	0.8	0.16	0.17
G020-024	6482	4.47	–1.90	1.5	0.77	–
G088-040	5928	4.14	–0.89	1.4	0.12	0.03
Giants						
BD-01°2916	4480[a]	1.2[a]	–1.99	2.4	0.39	0.16
BD+30°2611	4238	0.51[a]	–1.39	1.7	–0.01	–0.5
BD+54°1323	5213	2.01[c]	–1.64	1.5	–0.33	–0.21
BD+8°2856	4600[a]	0.8	–2.09	2.0	0.12	<0.73
CS31082-001[b]	4925	1.51[a]	–2.81	1.4	1.29	1.19
HD 74462[b]	4590	1.84	–1.48	1.1	0.13	–0.33
HD 83212	4530	1.21[a]	–1.25	1.8	–0.2	–0.53
HD 88609[b]	4568	1.01	–2.87	1.9	0.07	<0.25
HD 108317	5360	2.76[c]	–2.11	1.2	–0.08	0.15
HD 110184	4450[a]	0.5[a]	–2.40	2.1	0.22	0.15
HD 115444[b]	4785	1.5	–3.00	2.1	0.47	<0.35
HD 122563[b]	4560[a]	0.9[a]	–2.81	1.8	0.12	0.1
HD 122956	4700	1.51	–1.45	1.2	0.32	–0.28
HD 126238	4900	1.8	–1.92	1.5	0.24	–0.01
HD 126587	4700[a]	1.05[a]	–3.16	1.7	0.42	0.4
HD 128279	5200[a]	2.2[a]	–2.34	1.3	–0.16	–0.24
HD 165195	4200[c]	0.9[c]	–2.1	2.1	–0.32	–0.60
HD 166161[b]	5250[a]	2.15[c]	–1.25	1.9	0.0	0.05
HD 175305	5100	2.7	–1.38	1.2	0.04	0.04
HD 186478	4730	1.5[c]	–2.42	1.8	0.26	0.23
HD 204543	4700	0.8[a]	–1.84	2.0	0.04	0.04
HE0442-1234	4530	0.65	–2.32	1.8	0.12	–
HE1523-0901	4630[d]	1.00[d]	–2.95[d]	2.6[d]	1.2	1.4

Notes. [(a)] Stars with $T_{\rm eff}$ and log g derived from excitation potential and ionization balance. [(b)] Stars with an elemental r-process enhancement. [(c)] Stellar parameters were lowered in order to fulfil different criteria (see text). [(d)] values as derived in original paper (Frebel et al. 2007).